Angle-resolved photoemission spectroscopy with a femtosecond high harmonic light source using a two-dimensional imaging electron analyzer

S. Mathias
Department of Physics, University of Kaiserslautern, D-67663 Kaiserslautern, Germany

L. Miaja-Avila, M. M. Murnane, and H. Kapteyn
JILA, University of Colorado, Colorado 80309-0440, USA

M. Aeschlimann
Department of Physics, University of Kaiserslautern, D-67663 Kaiserslautern, Germany

M. Bauer
Institut für Experimentelle und Angewandte Physik, Christian-Albrechts-Universität zu Kiel, D-24908 Kiel, Germany

(Received 15 March 2007; accepted 27 July 2007; published online 23 August 2007)

An experimental setup for time- and angle-resolved photoemission spectroscopy using a femtosecond 1 kHz high harmonic light source and a two-dimensional electron analyzer for parallel energy and momentum detection is presented. A selection of the 27th harmonic (41.85 eV) from the harmonic spectrum of the light source is achieved with a multilayer Mo/Si double mirror monochromator. The extinction efficiency of the monochromator in selecting this harmonic is shown to be better than 7:1, while the transmitted bandwidth of the selected harmonic is capable of supporting temporal pulse widths as short as 3 fs. The recorded $E(k)$ photoelectron spectrum from a Cu(111) surface demonstrates an angular resolution of better than 0.6° (=0.03 $Å^{-1}$ at $E_{\mathrm{kin},e}$ =36 eV). Used in a pump-probe configuration, the described experimental setup represents a powerful experimental tool for studying the femtosecond dynamics of ultrafast surface processes in real time. © *2007 American Institute of Physics.* [DOI: 10.1063/1.2773783]

I. INTRODUCTION

In recording the momentum-resolved electronic structure $E(k)$ of a surface, angle-resolved photoemission spectroscopy (ARPES) has emerged as a leading experimental technique in identifying static key properties of complex systems such as adsorbed molecules[1] or high-temperature superconductors.[2] The ultrafast dynamics in these systems associated, for instance, with the nuclear motion or a phase transition after intense laser irradiation provide valuable information on fundamental physical properties. These ultrafast dynamics can, in principle, be mapped by the measurement of $E(k)$ as function of time using femtosecond time-resolved ARPES. In particular, by recording the energy distribution as well as the momentum distribution of the photoemitted electrons, a rather complete characterization of the different steps involved in these processes becomes possible. To drive such an experiment, powerful femtosecond and attosecond light sources in the extreme ultraviolet (EUV) regime are required, which have become available in recent years by means of high-order harmonic generation (HHG).[3–5,15] They have successfully been used in time-resolved PES for probing the ultrafast dynamics of gas-phase chemical reactions,[6] adsorbate-surface interactions,[7] or surface voltage transients.[8] The limitations in photon yield and repetition rate of these sources require, however, a highly efficient detection scheme for photoelectron spectroscopy.

In the past exclusively time of flight (ToF) electron analyzers have been used in PES experiments in combination with HHG because they exhibit a relatively high detection efficiency.[9–13] The drawback of these types of analyzers is their restricted energy resolution for kinetic electron energies beyond 10 eV, which is the energy regime typically probed in conventional EUV-PES. Furthermore, in their conventional configuration, these analyzers are only efficient in terms of energy detection. With respect to a mapping of the angular distribution of the photoemitted electrons only very specific and complex ToF configurations (for instance, multianode systems) can provide the required efficiency. To our knowledge, only one system worldwide, which was developed by Haight *et al.*,[14] has proven this performance, to date. For the realization of reasonable time- and angle-resolved PES (TR-ARPES), a parallel detection for energy and momentum of the photoemitted electrons is, however, indispensable. In recent years hemispherical energy analyzers have been developed which are equipped for the parallel (and therefore efficient) detection of a multitude of energy channels as well as momentum channels of the photoemitted electrons. This development has enabled an electron analyzer system for angle-resolved photoemission spectroscopy using a low-repetitive, low intensity HHG light source with high energy and high angular resolution independent of the electron kinetic energy.

The main challenge for this experiment is to show that ARPES at a reasonable countrate can be performed using a kilohertz fs-HHG source. In this article, we present the first ARPES data achieved with a 1 kHz HHG light source and

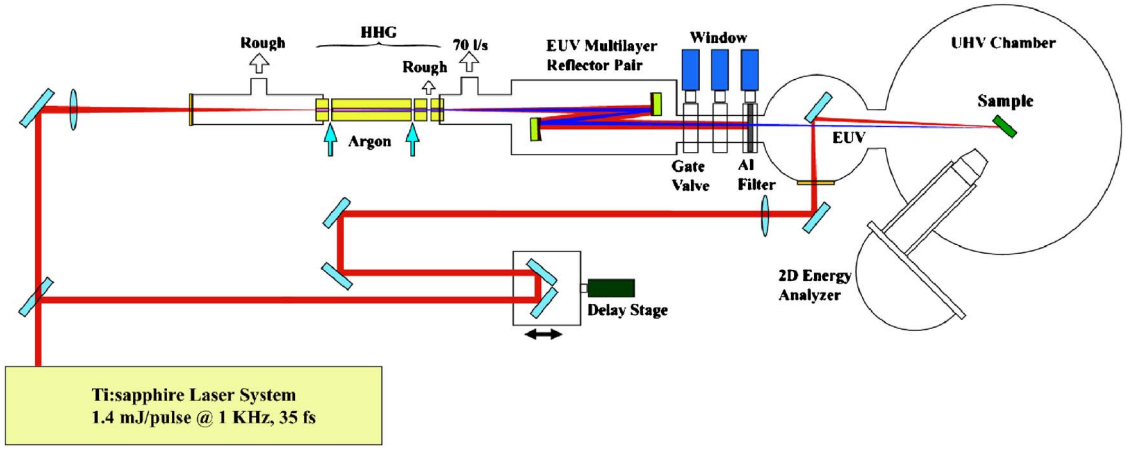

FIG. 1. (Color online) Experimental setup, consisting of a Ti:sapphire amplifier laser system, a HHG light source, a multilayer double mirror monochromator, and a 2D energy analyzer for parallel energy and momentum detection. For time-resolved pump-probe spectroscopy (not used in this work) part of the fundamental laser beam is separated with a beam splitter and is directly focused onto the sample after passing a computer-controlled optical delay stage.

using a hemispherical energy analyzer, equipped with a 2D detector for parallel energy and momentum detection. Our results show that ARPES using high harmonic light at a photon energy of 41.85 eV can be performed with an angular resolution better than 0.6° (corresponding to 0.03 $Å^{-1}$ at $E_{\mathrm{kin},e}=36$ eV). A comparison of the HHG PES spectra with corresponding data recorded with a conventional He discharge lamp ($h\nu=40.81$ eV) allows us to determine that the total bandwidth of the HHG light transmitted by the nondispersive monochromator is 801(10) meV, which is capable of supporting EUV pulses as short as 3 fs.

II. EXPERIMENTAL SETUP

In the following, we will first give a general overview of the experimental setup for fs-ARPES followed by a more detailed description of the two key features in Secs. II A and II B. A schematic view of the experimental setup is shown in Fig. 1. The high intensity laser system is a commercial 1 kHz multipass Ti:sapphire amplifier (Quantronics, "Odin") pumped by the second harmonic of a *Q*-switched Nd:YLF (yttrium lithium fluoride) laser (Quantronics model 527) and seeded by a sub-20 fs Ti:sapphire oscillator (KML-MTS kit). At an average power of 1.4 W, the amplifier produces 35 fs laser pulses with a central wavelength of 800 nm. The *p*-polarized amplifier output is split into pump and probe pulses, with 20% of the incident beam power in the pump pulse required for time-resolved experiments (not used in this study). The remaining 80% of the femtosecond laser light is used for the generation of the high harmonic probe pulse for photoelectron spectroscopy. This light is focused into an argon-gas-filled capillary (HHG light source, see Sec. II A) to generate ultrashort EUV pulses with energies up to 45 eV. A double mirror monochromator (see Sec. II B) consisting of two multilayer mirrors selects a single harmonic out of the discrete UV spectrum at a center photon energy of 41.85 eV. Furthermore, in order to focus the EUV light onto the sample surface, the second multilayer mirror is a concave mirror with a radius of curvature of 1 m. Residual light from the laser fundamental and low harmonics is filtered by a 200 nm thick aluminium film supported by a nickel mesh (Lebow) at the exit of the monochromator. The sample is mounted in an UHV chamber equipped with standard tools for surface preparation and characterization, such as sputter gun, e-beam heater, evaporator, low energy electron diffraction (LEED), and Auger. As a reference, the UHV chamber is also equipped with a gas-discharge VUV lamp (Focus model HIS 13) typically driven at 21 eV (He I) and 41 eV (He II). Furthermore, the fourth harmonic (6 eV) of the output of the Ti:sapphire oscillator has been used to record some of the photoemission spectra. The pressure in the UHV chamber rises to a value of about 5×10^{-10} mbar for experiments with the HHG light due to the noble gas load from the capillary cell. Photoemission spectra are recorded with a highly efficient hemispherical energy analyzer (SPECS Phoibos 150), equipped with a 2D detection unit for parallel energy and momentum detection.

The sample used for these studies is a Cu(111) crystal which has been cleaned by repeated Ar^+ sputtering (10 min, 500 V) and annealing cycles (15 min, 500 °C) prior to the experiments. Ultrathin silver films were evaporated at room temperature from a Knudsen-cell-type evaporation source at a rate of about 1 ML/min.

A. High-order harmonic light source

The HHG source used in this experiment is a three section hollow fiber setup for phase-matched generation of sub-10 fs EUV pulses.[15] The argon gas enters at the fiber intersections (marked by arrows in Fig. 1), which results in a constant gas pressure in the center part of the fiber. The small diameter of the inner core of 150 μm guarantees a high pressure gradient between the second capillary intersection and the UHV vacuum system and acts as a differential pumping stage. For HHG generation, the amplifier output is focused into the gas-filled fiber so that the laser beam is guided at high intensities through the hollow core over a total length of 10 cm. The large interaction length between the laser and argon gas, combined with phase-matching conditions achieved at proper gas pressures, leads to high conversion efficiencies into a coherent EUV beam. In our experiment, we used typical laser energies of 1 mJ/pulse. Phase-

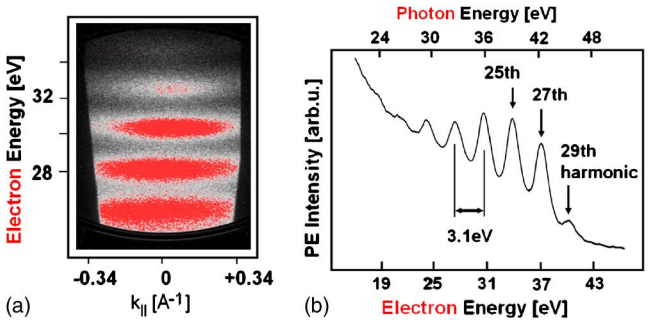

FIG. 2. (Color online) (a) Photoemission map recorded with fs-EUV light from a HHG capillary. No monochromator for harmonic selection was used, so that the electron energy distribution maps replicas of the Cu *d* bands for all harmonics transmitted through the HHG waveguide. (b) Corresponding energy distribution curve (EDC) at $k_{\|}=0$ Å^{-1}. The energy scale at the top of the graph (photon energy) is offset by the work function to show the energy of the incident harmonics.

matching conditions were achieved at an argon pressure of about 100 mbars in the capillary. High harmonic generation results from ionization, acceleration, and recollision of the outer electron in the gas atoms and results in a photon spectrum consisting of multiple harmonics of the fundamental frequency.[16,17] Because the nonlinear medium (argon) is centrosymmetric, even harmonics of the driving fundamental laser pulse are not present and only odd harmonics are observed in the HHG spectrum.

Figure 2 shows an $E(k_{\|})$ photoemission map (PE map) of the Cu(111) sample [Fig. 2(a)] and a corresponding energy distribution curve (EDC) at $k_{\|}=0$ Å^{-1} [Fig. 2(b)] recorded with the 2D-hemispherical energy analyzer under illumination with the HHG light and without a spectral selection by the monochromator described in the following section (however, with the aluminium filter inserted). The integration time for recording this spectrum was about 1 min. The spectrum shows several replicas of the Cu 3*d* bands resulting from the photoexcitation with different odd harmonic orders. This gives rise to an energy spacing of the *d*-band replicas of twice the fundamental photon energy (=3.1 eV). The high-energy cutoff of the spectrum, at about 45 eV photon energy, corresponds to photoemission by the 29th harmonic. This cutoff is mainly governed by the intensity of the laser pulse used for high harmonic generation.[18,19] The lack of any signal from harmonics below 25 eV (below the signal of the 19th harmonic) is due to absorption of EUV light by the argon gas in the HHG cell itself and absorption in the aluminium filter. The 27th harmonic ($h\nu=41.85$ eV) is clearly resolved in the EDC and exhibits sufficient photon flux ($\sim 10^6$ photons/pulse after 10% transmission due to the aluminium filter) for photoelectron spectroscopy.

B. The double mirror monochromator

For photoemission spectroscopy, a narrow photon energy is required with an energy width ideally much smaller than the feature of interest in the PE spectrum. Therefore, a finite energy range of the HHG-source spectrum has to be selected. However, the spectral bandwidth of the UV pulse determines its temporal width via the energy-bandwidth uncertainty product, and therefore limits the time resolution of a time-resolved PE experiment. A compromise between these two constraints (energy resolution and temporal resolution) must be found. Reflection gratings are the most common method of wavelength selection, where the gratings are arranged in a toroidal configuration that focuses the harmonic beam onto the sample. However, the diffraction of the harmonic light by the grating results in a tilt of the intensity distribution at a given time with respect to propagation direction leading to temporal broadening of the pulse.[20] Therefore, this approach is useful for situations where the harmonic radiation is used for static spectroscopy or when the dynamics of interest requires a time resolution not better than a few picoseconds. The use of a grating allows for an easy tunability of the EUV source over a wide photon energy range, which is particularly advantageous when compared with other selection techniques.

An alternative approach to restrict the spectral bandwidth of the harmonics is the use of VUV and EUV multilayer mirrors. These optics are equivalent to dielectric filters in the optical regime. They consist of a layered structure in which the optical constants vary periodically with depth, resulting in selective reflection of electromagnetic waves having particular wavelengths. In contrast to diffraction gratings, wavelength selection results from interaction with the periodicity perpendicular to the surface plane reflection in the zeroth order (specular reflection). Therefore, the outgoing ray does not exhibit the typical wave front tilting seen with conventional gratings, and temporal broadening of the reflected EUV pulse is not present.

In the present setup, multilayer mirrors consisting of a stack of 20 alternate layers of molybdenum and silicon are used. The mirrors have been manufactured for a maximum reflectivity at a wavelength of about 30 nm for near-normal incidence, which is close to the 27th harmonic of the 800 nm laser light. The reflectivity of the individual mirrors as function of wavelength has been measured for an incidence angle of 88°. These measurements agree rather well with calculated reflectivity data, following Ref. 21. For enhancement of the monochromator selectivity, we use a double multilayer mirror setup in a serial Z-folded design (see Fig. 1). Figure 3 shows the calculated total reflectivity for such a configuration at varying incidence angles in comparison to the harmonic peak spectrum. A maximum selectivity of the 27th harmonic is achieved for an incidence angle of about 85° with an overall reflectivity of 4%. This configuration of the monochromator predicts an extinction ratio of 45 with respect to the 25th harmonic and an extinction ratio of 10 with respect to the 29th harmonic. The expected bandwidth of the transmittance is about 2 eV [full width at half maximum (FWHM)], which is capable of supporting ultrashort pulses even for attosecond time-resolved spectroscopy.

A high momentum resolution in the photoemission experiment requires a small spot size of the EUV beam at the sample surface. In order to focus the EUV light onto the sample, the second mirror of the monochromator has a concave curvature with a radius of 1 m. The HHG light source and the sample surface are placed symmetrically at a distance of 1 m apart of the focusing mirror. For an estimated source diameter of the EUV light of about 100 μm and dif-

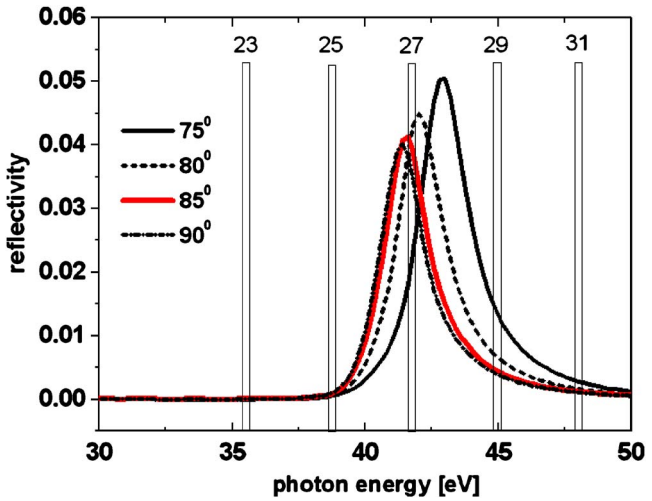

FIG. 3. (Color online) Calculated reflectivity of the double-mirror monochromator setup (Ref. 21). The red line corresponds to the experimental configuration (incidence angle of the harmonic light of 85°).

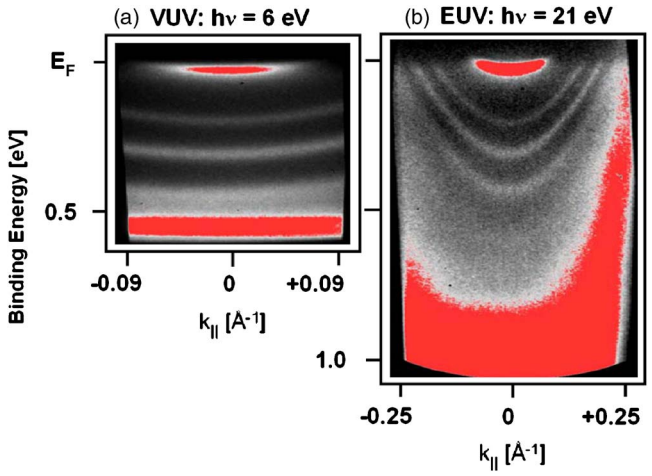

FIG. 4. (Color online) Angle-resolved PE spectra of the Shockley surface state and a series of quantum-well states of 40 ML Ag/Cu(111) recorded at photon energies of 6 eV [fourth harmonic of the Ti:sapphire oscillator, 4(a)] and 21.22 eV [He I line of the discharge VUV lamp (b)], respectively. An increase of the photon energy enables the access to electronic states at higher binding energies and extends the experimentally accessible momentum space.

fraction limited conditions,[8] this configuration gives rise to an effective spot diameter of 100 μm at the sample surface. For our analyzer settings, this value supports, in principle, to an angle resolution of 0.2°.

III. ANGLE-RESOLVED PHOTOEMISSION WITH HIGH HARMONICS

In comparison with femtosecond light sources in the visible or VUV regime, the use of high harmonic light for time-resolved experiments has three main advantages. (1) The high photon energies delivered by the HHG source extend the information accessible by time-resolved photoemission experiments to much deeper lying electronic states, even into the regime of classical core level spectroscopy. (2) The use of intense femtosecond pump pulses in time-resolved photoemission experiments often gives rise to a parasitic electron background in the kinetic energy range up to about 10 eV, resulting from multiphoton photoemission processes.[11,22] Therefore, to extract the relevant primary (probe) photoemission signal out of this background, the significantly higher photon energy (and consequently electron kinetic energy) delivered by a HHG source is desirable. (3) Finally, for a given acceptance angle of the energy analyzer, the use of high photon energies significantly extends the accessible momentum range of the photoemitted electrons. This last issue is highlighted in Fig. 4 which displays angle-resolved photoemission data of ultrathin silver films (40 ML) on Cu(111) recorded at photon energies of 6 eV [fourth harmonic of the Ti:sapphire oscillator, Fig. 4(a)] and 21.22 eV [He I line of the discharge VUV lamp, Fig. 4(b)], respectively. The plots map the kinetic energy distribution of the photoemitted electrons as function of the emission angle θ. The series of dispersive states visible in both maps are due to the Shockley surface state (topmost feature) and quantum well states (higher binding energy states); the latter ones localized within the silver film.[23,24] The component of the electron momentum parallel to the surface, $k_{\|}$, is conserved in the photoemission process, and for a given emission angle θ and kinetic energy E_{kin}, its absolute value can be calculated to

$$k_{\|} = \sqrt{\frac{2m_e}{\hbar^2} E_{\mathrm{kin}}} \sin(\theta). \tag{1}$$

This equation directly implies that for a given analyzer acceptance angle, a higher electron kinetic energy allows for a deeper view into momentum-space. The apparent difference in the dispersion of the quantum well states as function of emission angle between Figs. 4(a) and 4(b) is a direct consequence of this property. The constant acceptance angle of ±7° for both measurements transforms into a $k_{\|}$ interval of about ±0.09 Å^{-1} for initial state energies close to the Fermi edge at 6 eV excitation ($E_{\mathrm{kin},e} \approx 2$ eV) and into a $k_{\|}$ interval of about ±0.25 Å^{-1} for the same initial states but for excitation energies of 21 eV ($E_{\mathrm{kin},e} \approx 16$ eV). In terms of probing transient changes in $E(k)$ within a time-resolved photoemission experiment, the use of ultrashort EUV pulses instead of UV pulses will obviously extend the accessible states not only with respect to energy but also with respect to momentum.

A. ARPES using femtosecond high harmonic light

Figure 5 shows two photoemission maps of the Cu(111) surface for momentum values between 0.7 and 1.52 Å^{-1} (corresponding to electron emission angles between 13.3° and 28.3°). The left spectrum [Fig. 5(a)] has been recorded with the He II line of the gas-discharge lamp with a photon energy of $h\nu$=40.81 eV. The right spectrum [Fig. 5(b)] is the corresponding photoemission map recorded with the 27th harmonic with an energy of $h\nu$=41.85 eV. For both maps, identical analyzer settings have been used, corresponding to an energy resolution of 200 meV. Two dominant features can be identified in the two spectra: the barely dispersive copper 3*d* bands between 2 and 4 eV binding energy and the *sp* band which splits off the *d* band at about 0.85 Å^{-1} and which is characterized by its distinct parabolic dispersion. Contributions to the HHG spectrum due to lower and higher order

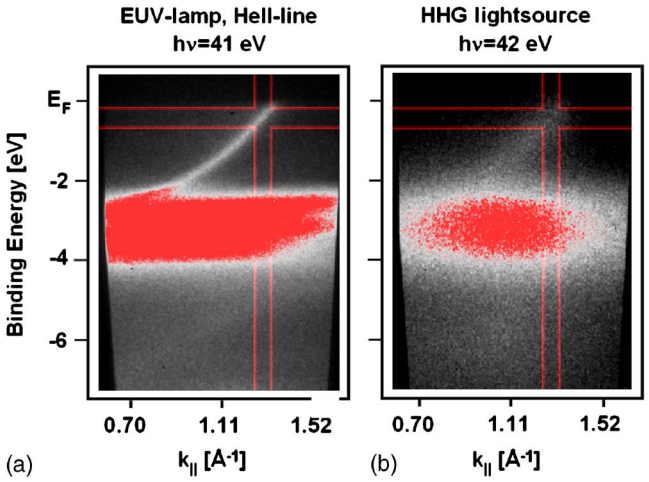

FIG. 5. (Color online) Photoemission maps of the Cu(111) *sp* band at finite angle with the He II line (a) and with the HHG light source, after selecting the 27th harmonic (b). The analyzer resolution was set to 200 meV. The HHG spectrum is broadened due to the energy bandwidth of 801(10) meV of the fs-HHG pulses. The red lines mark the integration areas for the energy and momentum distribution curves, as shown in Figs. 6 and 7. Note that there are no harmonic side bands observable.

harmonics (see, for reference, Fig. 2) are not visible in the spectrum. The upper limit of such a contribution can be deduced from the intensity ratio between the dominant *d*-band feature at 3 eV binding energy and the signal from the adjacent harmonics located at ±3.1 eV from this feature [see Fig. 6(a)]. From this estimation we find that any contribution from the 29th harmonic is suppressed by a ratio of better than 1:25, while the corresponding value for the 25th harmonic is better than 1:7. The increased suppression of the 29th harmonic in comparison to the measured/calculated multilayer mirror reflectivity is achieved by tuning the high-energy cutoff of the harmonic generation process right above the 27th order (see also the reduced intensity for the 29th harmonic in Fig. 2). The residual photon flux of the 27th harmonic available for photoemission spectroscopy after the aluminium filter and the monochromator is $\sim 8\times 10^3$ photons/pulse compared to $\sim 10^7$ photons/pulse delivered by the HHG light source.[25] Therefore, the integration time for the HHG spectrum is raised to about 50 min in comparison to 10 s for the conventional He II spectrum. Nevertheless, these spectra show that the used femtosecond high harmonic light source is suitable for reasonable mapping of the electronic band structure of a surface.

Evident, however, is an overall energy broadening of the photoemission features in the HHG spectrum in comparison to the He II spectrum. Due to the rather low HHG light intensity after the monochromator, the broadening cannot be attributed to space charge effects, as will be discussed in the following section. Therefore, the broadening only reflects the intrinsic bandwidth of the femtosecond HHG light pulses (time-bandwidth product for Gaussian-shaped and bandwidth-limited pulses ≈0.44). The achievable time resolution of a time-resolved ARPES experiment will be discussed in the following section. Furthermore, we will show that in comparison to the results obtained with the He II light source, the momentum resolution is not affected by the excitation with the HHG light (Sec. III C).

B. Energy distribution curves

EDC from the He II data and the HHG data as shown in Fig. 6(a) have been derived from the PE maps (Fig. 5) by a

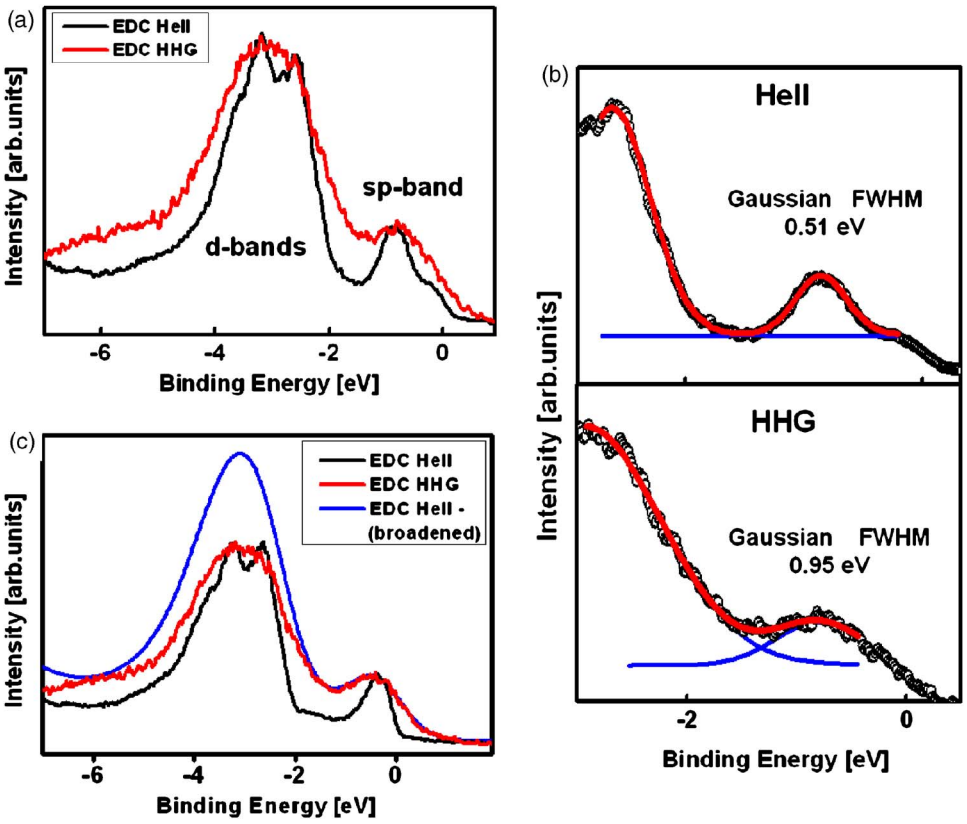

FIG. 6. (Color online) EDC (a) extracted from the photoemission maps in Fig. 5 ($k_{\|}$=1.15 Å^{-1}). (b) Gaussian fits of the *sp*-band peak. The deconvolution of the Gaussian of the *sp*-band peak in the HHG spectrum with the Gaussian linewidth of the *sp*-band peak in the He II spectrum gives a Gaussian bandwidth of 801(10) meV for the HHG light. (c) EDC extracted from the photoemission maps in Fig. 5 at a different $k_{\|}$ value ($k_{\|}$=1.25 Å^{-1}). The blue EDC is derived by convoluting the original He II spectrum with a Gaussian of 801 meV to mimic the broadening due to the bandwidth of the HHG light.

signal integration along $k_{\|}$, as indicated by the red marked area centered around $k_{\|}=1.15$ Å^{-1}. Both, *d* bands and *sp* bands are clearly resolved as peaks at about 3 eV binding energy and right at the Fermi level, respectively. All spectral features—*d* bands, *sp*-band peak, and Fermi edge—are strongly broadened in the HHG spectrum in comparison to the He II spectrum.

With the use of a low repetition, high intensity light source for photoemission spectroscopy, one must be aware of space charge effects leading to distortions in the photoemission spectrum. As a consequence of using pulsed radiation with high fluencies, the photomitted electrons leave the surface in short pulses with a fairly high electron density. Space charge effects due to the Coulomb repulsion between the electrons within such a pulse distort the spectral distribution of these electrons and result in a considerable loss in both energy resolution and angular resolution.[26,27] The strength of these distortions is goverened by the number of photoemitted electrons per area and pulse as well as the pulse length and the kinetic energy of the electrons.

A comparison of photoemission spectra recorded with different incident photon yields enables the quantification of space charge effects. A suitable reference spectrum in this context is the photoemission spectrum shown in Fig. 2, which has been recorded without the monochromator installed. The number *N* of photoemitted electrons per pulse and area *A* in this experiment is about two orders of magnitude larger than in the experiments done with the monochromator (see Fig. 6). The difference (quadratic subtraction) of the width of the *d*-band feature in both spectra is, however, less than 500 meV. Based on this result we can give an upper value for the space charge broadening in the spectra recorded with the monochromator following the $\sqrt{N}/\sqrt{A}$ dependence, as given in Ref. 26. We find that the maximum contribution to the energy broadening for the experiments with a single harmonic is 56 meV. The quadratic addition of this value to the intrinsic linewidth of *d* band and *sp*-band feature as deduced from the He II spectrum results in a line broadening of the peak FWHM well below 5 meV, a value that cannot be resolved with the analyzer settings (pass energy) used in the experiments.

The comparison of the *sp*-band peak width of the He II and the HHG spectrum can therefore be used to determine the bandwidth of the EUV pulse. For both spectra we performed Gaussian fits to the *sp*-band peak and determined the corresponding peak FWHM [see Fig. 6(b)]. Quadratic subtraction of the He II-spectrum FWHM from the HHG-spectrum FWHM gives the lower limit for the spectral bandwidth of the HHG radiation. This value is equal to the HHG bandwidth, for the case that the contribution of the linewidth of the He II light to the spectral broadening of the EDC is negligible. For the He II *sp*-band peak, we measure a FWHM of 0.51 eV in comparison to 0.95 eV derived from the HHG spectrum. This gives a bandwidth value for the HHG radiation of 0.801(10) eV. To verify the validity of this approach, we convolved the He II EDC at a different $k_{\|}$ ($k_{\|}=1.25$ Å^{-1}), with a Gaussian representing the HHG spectra distribution with the derived bandwidth of 801 meV. A comparison of the resulting EDC with the corresponding HHG EDC is shown in Fig. 6(c). The convolution result matches perfectly the measured Fermi-edge distribution and the *sp*-band peak [blue line in Fig. 6(c)]. The differences in the *d*-band peak between convoluted EDC and the measured HHG-EDC can be assigned to the different polarizations of the two light sources used in the experiment (unpolarized for the discharge lamp and *p*-polarized for the HHG light) due to polarization and state sensitive transition matrix elements.

The bandwidth of the EUV-HHG pulses of 801(10) meV is capable of supporting a temporal pulse width of 3 fs. This value is the upper limit of time resolution achievable in a pump-probe experiment using the described HHG beam line. Since there are no further dispersive elements in the beam line, we assume (without measurement) that this pulse length is actually operative in our experiment. Using chirped or shaped laser pulses should further narrow the HHG bandwidth in the future,[28] although higher pulse energies would be needed to maintain the same intensity for HHG generation.

C. Momentum distribution curves

Figure 7 shows the momentum distribution curves (MDCs) derived from the red marked areas of Fig. 5 at an energy just below the Fermi level. As was the case for the EDC, we observe a clear broadening in comparison to the He II-MDC. In the following we will show that this broadening is related to the energy broadening of the PE spectrum by the bandwidth of the HHG radiation and that the momentum resolution is not affected by the use of the femtosecond HHG pulse. Let us first consider the momentum spread in the PE spectrum due the momentum vector of the HHG light itself. The total momentum added by the absorption of a 42 eV photons to an electron is about 0.02 A^{-1}. The momentum spread delivered by the different frequency components contributing to the selected harmonic is consequently much smaller (0.0004 A^{-1} for 801 meV bandwidth) and therefore cannot account for the observed broadening of the HHG-MDC. Another point to consider with respect to momentum resolution is the spot size of the EUV light at the surface determining the source diameter for photoemitted electrons. In our setup, the HHG light is focused by the second mirror of the monochromator to a spot size of about 100 μm to guarantee a high angular resolution (see Sec. II B). By comparison, the He II light is not focused onto the sample and exhibits a beam diameter of 600 μm. Therefore, the spot size cannot account for the broadening of the MDC trace, either. To check to what extent the spectral energy broadening due to the finite bandwidth of the HHG affects the MDC, we performed the following convolution procedure. EDCs for a series of $k_{\|}$ values measured with the He II lamp were convolved with a 801 meV Gaussian to mimic again the energy broadening of the HHG EDCs (see Sec. III B). From these EDC series we then extract a purely "energy broadened" MDC and compare this spectrum with the measured HHG-MDC (see Fig. 7). Evidently the simulated and measured MDCs agree almost perfectly. We therefore conclude that the use of the HHG light source does not degrade the momentum resolution of the ARPES experiment.

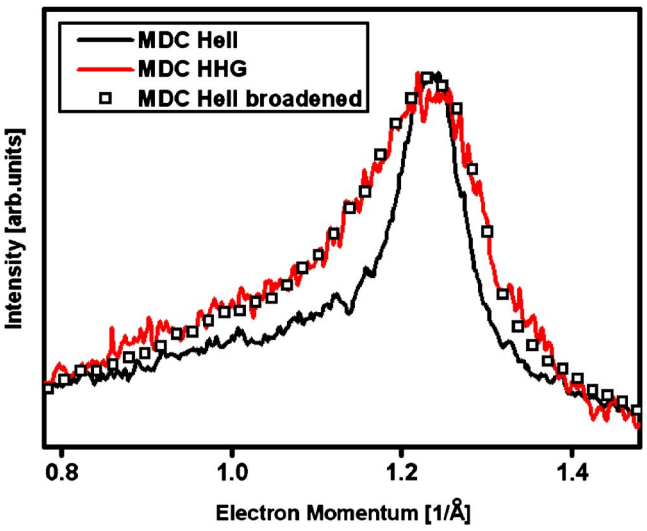

FIG. 7. (Color online) Momentum distribution curves (MDCs) extracted from the photoemission maps in Fig. 5. The MDC marked by open squares was derived after convoluting the He II EDCs with the HHG bandwidth of 801 meV for all different $k_{\parallel}$ values (see text).

A detailed specification of the analyzer momentum resolution using the He discharge lamp (beam diameter of 600 μm) shows an effective angle resolution of 0.6°, corresponding to a momentum resolution of 0.03 $Å^{-1}$ at a kinetic energy of 36 eV. Due to the smaller HHG spot size in comparison to the He II light, we expect that the angular resolution in the HHG experiment even exceeds this value.

IV. DISCUSSION AND OUTLOOK

In summary, we presented angle-resolved photoemission spectra recorded by excitation with femtosecond high harmonic light and using a 2D imaging energy analyzer for parallel energy and momentum detection. To select a single harmonic from the harmonic spectrum, a specifically designed monochromator consisting of a pair of Si/Mo multilayer mirrors has been used. The extinction efficiency of the monochromator with respect to neighboring harmonic satellites is shown to be better than 7:1. The bandwidth of the transmitted EUV light is 801(10) meV, and thus broad enough to support pulses as short as 3 fs. The use of a curved multilayer mirror in the monochromator guarantees a focusing of the HHG light onto the surface and a correspondingly small spot size. By this means an angular resolution in the HHG photoemission experiment of better than <0.03 $Å^{-1}$ could be achieved. Yet, the relatively long integration times required to record a complete photoemission map are somewhat unsatisfactory. This constraint can, however, be overcome by some modifications in the experimental setup. Femtosecond amplifier systems with equivalent pulse specifications as the system used in this work but driven at repetition rates as high as 20 kHz are commercially available and will reduce typical measurement times by a factor of 20. Furthermore, quasi-phase-matching conditions for HHG generation can be achieved by the use of periodically modulated fibers[29] or counterpropagating light[30] and give rise to significantly enhanced EUV photon fluxes. The spectral bandwidth of the harmonics can also be reduced by using narrower mirrors, chirped or shaped pulses.

Finally, we would like to emphasize the advantage of the parallel use of the He II light source and the HHG EUV light source for ARPES experiments. The latter light source will allow for time-domain measurements at exceptionally high temporal resolution to map ultrafast transient changes in the $E(k)$ distribution. The former light source can support these experiments by high resolution spectroscopy in the frequency
domain.

Future prospects of time-resolved ARPES include studies of ultrafast processes of systems characterized by transient changes in the electronic structure $E(k)$. This may include, for instance, the ultrafast dynamics associated with highly correlated systems such as high-temperature superconductors, the interaction of adsorbates and surfaces, or the dynamics of phase transitions such as laser-induced melting processes in conventional metals.

ACKNOWLEDGMENTS

This work was supported by the Deutsche Forschungsgemeinschaft through SPP 1093 and the Stiftung Innovation RLP. Special thanks go to Yanwei Liu and Chi-Fong Lei for providing the EUV multilayer mirrors. One of the authors (L.M.A.) acknowledges support from the NSF.

[1] H.-P. Steinrück, J. Phys.: Condens. Matter **8**, 6465 (1996).
[2] A. Damascelli, Z. Hussain, and Z. X. Shen, Rev. Mod. Phys. **75**, 473 (2003).
[3] Ch. Spielmann *et al.*, Science **278**, 661 (1997).
[4] P.-M. Paul, E.-S. Toma, P. Breger, G. Mullot, F. Auge, P. Balcou, H.-G. Muller, and P. Agostini, Science **292**, 1689 (2001).
[5] M. Hentschel *et al.*, Nature (London) **414**, 509 (2001).
[6] L. Nugent-Glandorf, M. Scheer, D. A. Samuels, A. M. Mulhisen, E. R. Grant, X. Yang, V. M. Bierbaum, and S. R. Leone, Phys. Rev. Lett. **87**, 193002 (2001).
[7] M. Bauer, C. Lei, K. Read, R. Tobey, J. Gland, M. M. Murnane, and H. C. Kapteyn, Phys. Rev. Lett. **87**, 025501 (2001).
[8] P. Siffalovic, M. Drescher, and U. Heinzmann, Europhys. Lett. **60**, 924 (2002).
[9] M. Bauer, C. Lei, R. Tobey, M. M. Murnane, and H. Kapteyn, Surf. Sci. **532–535**, 1159 (2003).
[10] L. Nugent-Glandorf, M. Scheer, D. A. Samuels, V. Bierbaum, and S. R. Leone, Rev. Sci. Instrum. **73**, 1875 (2002).
[11] P. Sifflacovic, M. Drescher, M. Spieweck, T. Wiesenthal, Y. C. Lim, R. Weidner, A. Elizarov, and U. Heinzmann, Rev. Sci. Instrum. **72**, 30 (2001).
[12] G. Tsimilis, J. Kutzner, and H. Zacharias, Appl. Phys. A: Mater. Sci. Process. **76**, 743 (2003).
[13] L. Miaja-Avila, C. Lei, M. Aeschlimann, J. L. Gland, M. M. Murnane, H. C. Kapteyn, and G. Saathoff, Phys. Rev. Lett. **97**, 113604 (2006).
[14] R. Haight, J. A. Silberman, and M. I. Lilie, Rev. Sci. Instrum. **59**, 1941 (1989).
[15] Rundquist, C. G. Durfee III, Z. Chang, C. Herne, S. Backus, M. M. Murnane, and H. C. Kapteyn, Science **280**, 1412 (1998).
[16] A. McPherson, G. Gibson, H. Jara, U. Johann, T. S. Luk, I. McIntyre, K. Boyer, and C. K. Rhodes, J. Opt. Soc. Am. B **4**, 825 (1987).
[17] M. Ferray, A. L'Huillier, X. F. Li, L. A. Lompré, G. Mainfray, and C. Manus, J. Phys. B **21**, L31 (1988).
[18] J. L. Krause, K. J. Schafer, and K. C. Kulander, Phys. Rev. Lett. **68**, 3535 (1992).
[19] P. B. Corkum, Phys. Rev. Lett. **71**, 1994 (1993).
[20] P. Villoresi, Appl. Opt. **38**, 6040 (1999).
[21] http://www.cxro.lbl.gov

[22] M. Bauer, J. Phys. D **38**, R253 (2005).
[23] T. C. Chiang, Surf. Sci. Rep. **39**, 181 (2000).
[24] S. Mathias, M. Wiesenmayer, M. Aeschlimann, and M. Bauer, Phys. Rev. Lett. **97**, 236809 (2006).
[25] The HHG light source delivers $\sim 10^7$ photons/pulse. The aluminium filter reduces the flux by a factor of 10. The double mirror monochromator selects the 27th harmonic and additionally reduces the flux by about a factor of 5. The overall transmission of the 27th harmonic by the two mirrors is 4%. Residual intensity is therefore $\sim 8 \times 10^3$ photons/pulse.
[26] S. Passlack, S. Mathias, O. Andreyev, D. Mittnacht, M. Aeschlimann, and M. Bauer, J. Appl. Phys. **100**, 024912 (2006).
[27] X. J. Zhou *et al.*, J. Electron Spectrosc. Relat. Phenom. **142**, 27 (2005).
[28] R. A. Bartels, S. Backus, I. P. Christov, H. C. Kapteyn, and M. M. Murnane, Chem. Phys. **267**, 277 (2001).
[29] A. Paul *et al.*, Nature (London) **421**, 51 (2004).
[30] X. Zhang, A. L. Lytle, T. Popmintchev, X. Zhou, H. C. Kapteyn, M. M. Murnane, and O. Cohen, Nat. Phys. **3**, 270 (2007).